International Journal of Heat and Mass Transfer 169 (2021) 120906

Contents lists available at ScienceDirect

International Journal of Heat and Mass Transfer

journal homepage: www.elsevier.com/locate/hmt

Heat transfer and friction in a high aspect ratio rectangular channel with angled and intersecting ribs

Giovanni Tanda*, Francesca Satta

DIME, Università degli Studi di Genova, via Montallegro 1, I-16145 Genova, Italy

ARTICLE INFO

Article history:
Received 20 August 2020
Revised 14 December 2020
Accepted 2 January 2021

Keywords:
Ribbed channel
Heat transfer enhancement
Angled rib
Intersecting rib
Liquid crystals

ABSTRACT

Forced convection heat transfer in a high aspect ratio (5:1) rectangular channel with 45 deg angled ribs has been investigated. The ribs are periodically positioned on one wall of the channel, heated at uniform heat flux over each inter-rib region. In the pursuit of heat transfer enhancement, longitudinal ribs (termed intersecting ribs), oriented parallel to the mainstream, have been added to the angled ribs. Friction and heat transfer characteristics were determined for two values (10000 and 20000) of the Reynolds number. Liquid crystal thermography was employed as diagnostic tool in heat transfer experiments. The study was supplemented with CFD numerical calculations using the RNG k-ε turbulence model. Local and regionally averaged heat transfer and flow characteristics of the tested rib configurations have been presented and compared. Both experimental and numerical results were able to capture the effect produced by the intersecting ribs on vortices and their ability to locally increase the heat transfer coefficient and promote its more uniform distribution. If the standard angled rib configuration is assumed to be the reference condition, the thermal performance based on the same pumping power is increased in the case of the insertion of one intersecting rib, while two intersecting ribs are unable to provide further enhancements.

1. Introduction

Artificial roughened channels are considered to be an effective way to improve the thermal performance in a large variety of engineering applications such as internal cooling of gas turbine blades [1], solar air heater ducts [2], microelectronic equipment cooling [3], and high-temperature heat exchangers [4] and combustors [5]. The effect of rib turbulators has been studied by many scientists; attention has been paid to many parameters of ribbed channel, such as rib shape, channel aspect ratio, rib pitch-to-height ratio, rib blockage ratio, rib angle of attack and so on. Since roughening the walls of a channel typically produces higher heat transfer coefficients and higher pressure losses, the evaluation of advantages of using rib-roughened channels must include not only the heat transfer augmentation induced by ribs, but also the friction factor increase and the thermal performance, which compares the heat transfer augmentation, relative to a reference condition (e.g., a smooth channel), for the same pumping power. Based on the extended literature review performed by Han et al. [1], angled ribs were found to provide higher thermal performance than the transverse ribs due to the rib-angle-induced secondary flow. However, angling the ribs is more effective for channels with a narrow aspect ratio (e.g., AR = ¼ or ½), which provide similar or slightly higher pressure drop as compared with transverse ribs but significantly higher heat transfer coefficients [6–10]. Conversely, when the channel aspect ratio is relatively large (e.g., AR = 2 or more) the effect of the secondary flow induced by the rib inclination diminishes since the two opposite ribbed walls are too close to each other, so that the heat transfer enhancement is limited; the same considerations apply when ribs are deployed on one side only. Thus, for high aspect ratio channels, the identification of improved rib configurations able to significantly enhance thermal performance is strongly desirable. The solutions investigated in the literature to promote higher thermal performance in high aspect ratio channels with angled ribs include: angled-crossed ribs, V-shaped and W-shaped continuous, multiple, and broken (or discrete) ribs, angled broken ribs, angled ribs with a gap, angled ribs with longitudinal intersecting ribs. A pictorial top view of some of these high-performance rib configurations is shown in Fig. 1.

1.1. Angled-crossed ribs

Han et al. [11] experimentally investigated heat transfer performance, relative to that of a smooth channel, for several types of ribs placed on two opposite walls of a square channel (AR= 1); they found that the crossed rib configuration had the lowest heat transfer enhancement and the smallest pressure drop penalty.

* Corresponding author.
E-mail address: giovanni.tanda@unige.it (G. Tanda).

https://doi.org/10.1016/j.ijheatmasstransfer.2021.120906
0017-9310/

Nomenclature

AR	channel aspect ratio (-)
D	channel hydraulic diameter (m)
e	rib height (m)
f	friction factor (-)
f_b	friction factor for the baseline rib configuration (-)
H	channel height (m)
h	heat transfer coefficient (W $m^{-2}K^{-1}$)
k	air thermal conductivity (W $m^{-1}K^{-1}$)
L	ribbed channel length (m)
Nu	Nusselt number (-)
Nu_b	Nusselt number for the baseline rib configuration (-)
$\overline{Nu}$	regionally averaged Nusselt number (-)
$\overline{Nu}_b$	regionally averaged Nusselt number for the baseline rib configuration (-)
P	pressure (Pa)
p	rib pitch (m)
q_{conv}	convective heat flux (W m^{-2})
Re	Reynolds number (-)
T_{air}	air bulk temperature (K)
T_w	wall temperature (K)
U	mean air velocity (m s^{-1})
W	channel width (m)
x,y	streamwise and transverse coordinates (m)
Greek symbols	
η	thermal performance index, Eq. (5) (-)
ν	air kinematic viscosity (m^2 s^{-1})
ρ	air density (kg m^{-3})

This result was confirmed by Won and Ligrani [12], who compared the flow structure and local heat transfer coefficients in a high aspect ratio channel ($AR = 4$) with parallel and crossed ribs, inclined at 45 deg. When viewed in flow cross-sectional planes, the secondary flow structure generated by the crossed ribs contains a single cell of fluid, whereas the parallel-rib arrangement induces two cells of large-scale motion. Heat transfer coefficients were roughly the same for the crossed and parallel rib configurations for all locations along the test surface, except just upstream of the ribs, where the parallel rib configuration performed better.

1.2. V-shaped and W-shaped ribs

The search for high-performance ribs included V-shaped and W-shaped arrangements [13–19]. The effects of V-shaped continuous ribs pointing upstream and downstream [13,14,16], V-shaped continuous, multiple or discrete ribs [15,17–19], and W-shaped continuous and discrete ribs [18] have been investigated, encompassing a range of channel aspect ratio from 1 up to 8. Superior thermal performance of V-shaped ribs, relative to standard angled ribs, is generally recognized. Gao and Sundén [16] found that, for a high aspect ratio stationary channel ($AR = 8$), the V-ribs pointing downstream produced higher heat transfer enhancement, friction factors and thermal performance than the V-ribs pointing upstream, over the tested Reynolds number range. Systematic experiments performed by Wright et al. [18] on a large variety of high-performance ribs, for a high aspect ratio stationary and rotating channel ($AR = 4$), showed that the discrete V-shaped ribs and the discrete W-shaped ribs provide the best thermal performance.

1.3. Angled broken ribs

An alternative strategy to improve the thermal performance of standard angled ribs consists in truncating the ribs to induce more local wall turbulence. Han and Zhang [20] investigated the thermal performance of angled broken and V-shaped broken ribs inside square channels ($AR = 1$). The Nusselt number for 60 and 45 deg angled broken ribs or V-shaped broken ribs were much higher than the corresponding 60 and 45 deg angled or V-shaped continuous ribs, while the corresponding friction factors were comparable with each other for broken and continuous rib configurations. Discrete ribs obtained dividing each continuous, 45 deg, angled rib into two, three, or five pieces were studied by Cho et al. [21], for a channel aspect ratio of 2.04. Discrete ribs provided heat/mass transfer performance lower or comparable with that of the angled continuous ribs, regardless of the number of broken pieces, but their use led to a uniformity of the heat/mass transfer coefficient distribution that increases with the number of discrete ribs.

1.4. Angled ribs with a gap

Augmentation of thermal performance can be provided by considering a single gap in the inclined ribs, as reported in [22–24]. Cho et al. [22] examined the effect of a gap in ribs with an angle of attack of 60 deg for a square channel ($AR = 1$). Two different gap positions (upstream and downstream gaps) were considered. The gap was found to promote flow mixing and turbulence with higher heat transfer coefficients and similar or slightly lower friction losses than those for the continuous rib configurations; the rib configurations with the gap located downstream showed slightly higher heat transfer enhancements than the upstream gap rib arrangements. Aharwal et al. [23] carried out a systematic study aimed at optimizing the position and width of the gap for inclined ribs. Experiments were performed in a rectangular channel with a high aspect ratio ($AR = 5.83$) having the ribs installed on one side, and for different values of Reynolds number, rib pitch-to-height ratio, relative roughness height, and rib angle. The maximum benefit was achieved at a gap position about one fourth of the duct width, corresponding to the region of relatively low heat transfer induced by the rib inclination: here the secondary flow carrying relatively warm fluid along the rib is mixed with the main flow passing through the gap, leading to a local heat transfer enhancement. Chaube et al. [24] experimentally investigated heat transfer and friction in a square channel ($AR = 1$) with angled ribs with a gap, by varying the rib angle and the relative gap position and width: the maximum heat transfer and friction factor enhancement were found to occur at the relative gap position of one third with relative gap width of one and for rib attack angle of 60 deg.

1.5. Angled ribs with longitudinal intersecting ribs

A recent and innovative proposal to improve the thermal performance of angled ribs in large aspect ratio channels consists in applying one or more longitudinal ribs to intersect the angled ribs. The main purpose of the intersecting rib is to promote additional vortices to be generated at the points of intersection with the angled ribs. This type of enhanced rib configuration was first documented by Chung et al. [25], who investigated the effect on thermal performance of a longitudinal rib that bisects 60 deg angled ribs. Experiments were performed for rectangular channels (AR from 1 to 4) ribbed on two opposite channel walls, by using the naphthalene sublimation technique. The most interesting finding was that the installation of one longitudinal rib increases the thermal performance, for any aspect ratio and Reynolds number. The thermal performance enhancement, relative to the standard angled rib configuration, was found to be larger, on percentage,

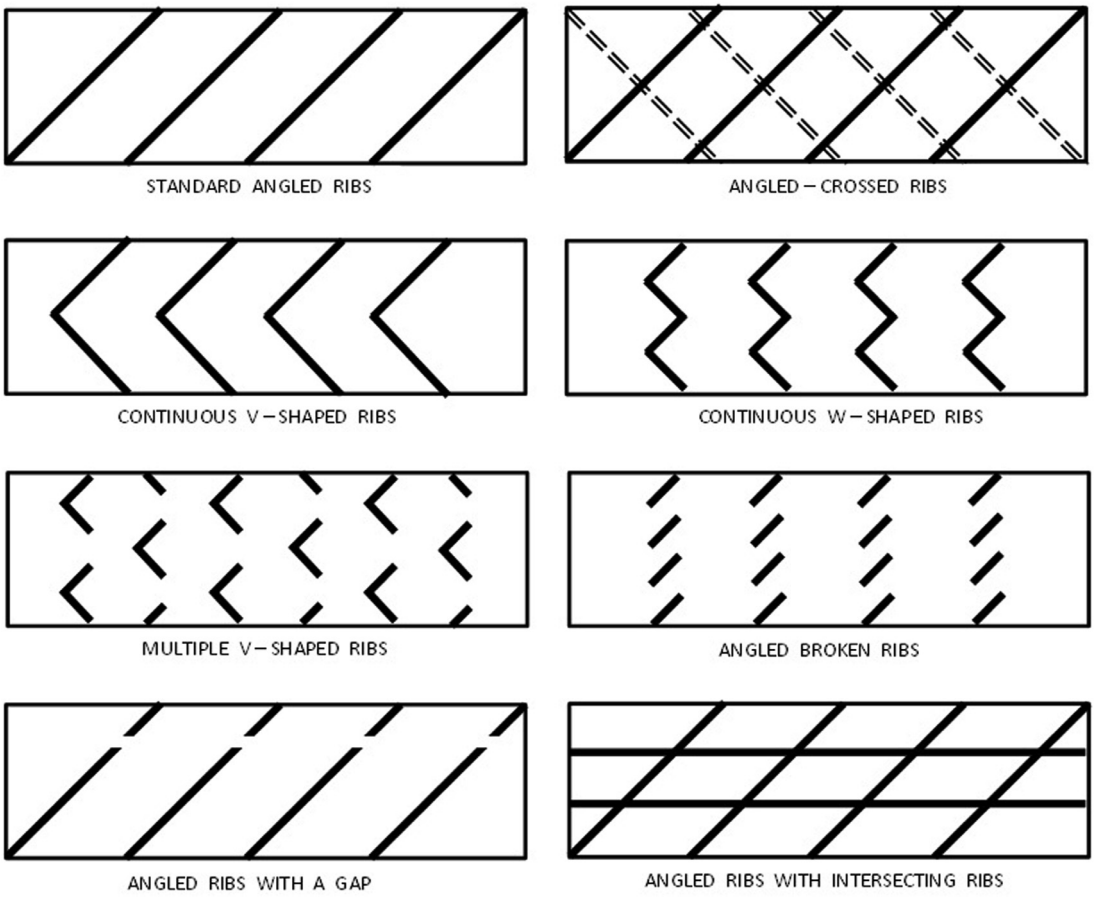

Fig. 1. Top view of some high-performance rib configurations.

at the highest aspect ratios (AR = 2 and 4). According to Chung et al. [25], further performance improvements for the largest channel aspect ratio (AR = 4) could be potentially expected by installing more intersecting ribs. Recently, Afzal et al. [26] applied a neural-network-assisted numerical optimization technique, coupled with computational fluid dynamics, to identify optimal conditions for rectangular channels with angled and intersecting ribs and aspect ratios equal to 1, 2, and 4. Three design variables (rib angle of attack, ratio of the intersecting rib location relative to the channel center-line to channel width, and ratio of rib height to hydraulic diameter) were selected for optimization to maximize the thermal performance. A relative increase of 14.4, 12.8, and 16.2% in thermal efficiency (compared to the standard angled ribs) was found for AR =1, 2, and 4, respectively, with an optimal rib angle in the 38−50 deg range. As AR was increased from 1 to 4, the position of the intersecting rib (relative to the channel center-line) and the rib height-to-hydraulic diameter ratio varied from 0.21 to −0.11 and from 0.049 to 0.085, respectively.

The present study focuses on heat transfer and friction characteristics of a high aspect ratio (AR = 5) rectangular channel with 45-deg angled ribs, deployed on one side only, and coupled with one or two longitudinal, intersecting ribs. The aim of this research was to experimentally evaluate the potential for enhancing the thermal performance of the ribbed channel provided by the insertion of longitudinal ribs, taking the standard angled rib as the baseline, reference configuration. Detailed local and regionally averaged heat transfer coefficients, derived from liquid crystal thermographic experiments, are presented and discussed. Experiments have been complemented with numerical simulations and results have been processed to obtain the thermal performance of the channel, inclusive of the pressure drop penalties.

2. The experimental apparatus

Fig. 2 shows the sketch of the experimental apparatus. Air at room temperature was drawn by a blower into a plenum, from which it passed successively through a filter, a contraction, the entrance section, the test section (pictured in the insets of Fig. 2), and a re-development section. From there, air is discharged out of the laboratory room.

The entrance (or development) section, 0.02 m high and 0.1 m wide, served to establish hydrodynamically fully developed flow at the test section inlet. The test section was a rectangular channel, having the same cross section of the entrance channel (height H = 0.02 m, width W = 0.1 m, aspect ratio $AR = W/H$ = 5, hydraulic diameter D = 0.033 m) and a length L = 1.124 m. Square ribs (height e = 0.003 m, rib height-to-hydraulic diameter ratio e/D = 0.09), angled at a 45 deg angle with respect to the longitudinal direction, were periodically glued on the lower wall of the channel. The rib pitch p was 0.03 m, with a rib pitch-to-height ratio p/e equal to 10. The opposite wall and the side walls were smooth and made of Plexiglas. The first 18 inter-rib modules of the ribbed wall were unheated, while the last 16 inter-rib modules were heated at uniform heat flux by means of a plane heater, as indicated in Fig. 2.

The rib configurations tested in this study are shown in Fig. 3. The baseline configuration consisted of ribs angled at 45 deg. The second rib configuration was implemented by a longitudinal rib positioned in the midline of the ribbed surface. In the last rib configuration, two longitudinal ribs have been added to the ribbed surface at one third and two thirds of its width, respectively. The presence of the longitudinal ribs (also named intersecting ribs) was expected to significantly affect the secondary flow and the distri-

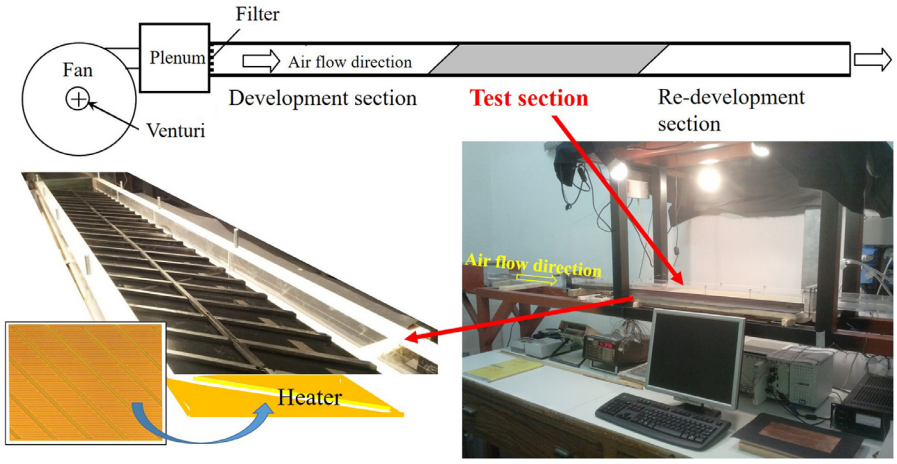

Fig. 2. Sketch and photographic illustrations of the experimental setup.

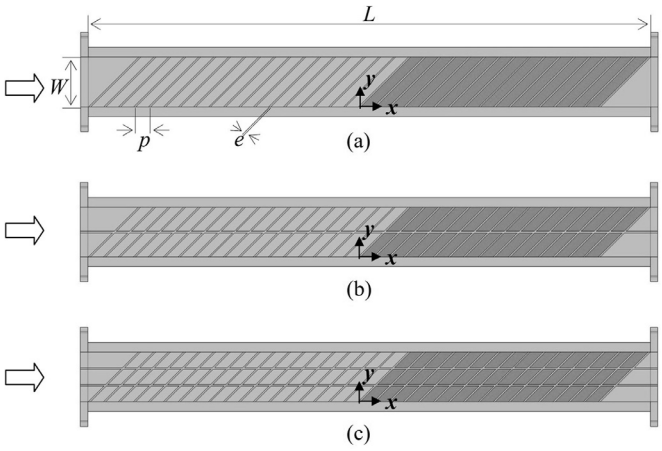

Fig. 3. Test section with the three rib configurations: (a) standard angled ribs, (b) angled ribs with one central intersecting rib, (c) angled ribs with two equally spaced intersecting ribs. Unheated and heated ribbed regions are displayed with a different grey scale (light grey is used for unheated regions).

bution of heat transfer coefficient with respect to the baseline rib configuration.

The heater employed to provide uniform heat flux conditions over each inter-rib surface region consisted of a properly designed printed circuit board (a copper track deposited onto a Vetronite thin sheet), composed by 16 rhomboidal modules connected in series leaving unheated the baseplate of each rib. This was made in order to precisely estimate the heat flux effectively delivered to each inter-rib region; on the other hand, tangential conduction towards the unheated fiberglass strips covered by ribs probably may lead to a local overestimation of heat transfer coefficient immediately upstream and downstream of each rib. Further details of the printed circuit board adopted in the present experiments are given in Ref. [27].

The steady-state, liquid crystal (LC) technique was chosen to measure the local wall temperature and finally to calculate the heat transfer coefficient, as it was successfully applied by this research group in similar experimental studies [17,27–30]. A prepackaged LC sheet (R30C5W, Hallcrest), 0.15 mm thick, consisting of a liquid crystal layer sandwiched between a thin Mylar film and a black backing coating, was glued onto each inter-rib module of the heated test section. The color distribution of the LCs was taken by a Nikon D-70 camera through the Plexiglas wall opposite to the ribbed heated surface. Four LED (light emitting diodes)-based light sources (color temperature of 3000 K) were used to provide a uniform lighting of the heated test section. The LC sheet was calibrated by a dedicated experiment in order to infer the relationship between hue and temperature, as reported in Ref. [27]. LC images gathered during the experiments in the ribbed channel were processed to obtain the wall temperature from the hue distribution. A convolution filter was used to minimize the effects of image defects producing, in isolated pixels, values of hue not correlated to the surface temperature. After resizing and filtering processes the resolution was about 0.5 mm/pixel.

Several fine-gauge thermocouples were employed for measuring the temperature of air entering the test section and controlling the attainment of the steady-state conditions. The mass flow rate was measured by means of a Venturi flowmeter, placed upstream of the blower. Static pressure taps, distributed along the streamwise direction, provided pressure drop data.

3. The experimental procedure and data reduction

For a prescribed air mass flow rate, a given heat flux was induced by adjusting the electric power supplied to the printed circuit board, until the colors exhibited by LCs were observed over the area of interest. At thermal equilibrium, the LC image was taken, stored, and processed to obtain the map of surface temperature from values of hue. The local heat transfer coefficient h is determined from

$$h = q_{conv}/(T_w - T_{air}) \tag{1}$$

where q_{conv} is the convective heat flux, T_w is the wall temperature deduced from LCs (and corrected on the basis of the thermal resistance introduced by the thin Mylar coating), and T_{air} is the air bulk temperature. The local bulk temperature of air T_{air} was calculated from the measured inlet temperature and the net heat input to the air flow using the conservation of energy principle (the discontinuity in the heat input in correspondence to each unheated rib was accounted for). The convective heat flux q_{conv} was evaluated subtracting the heat flux losses by radiation and conduction to the measured electrical heat flux (i.e., the input power delivered to the heater divided by the heat transfer area). The radiative heat losses were calculated by considering a diffuse gray-surface network, while the conductive heat losses were calculated by using a one-dimensional conduction analysis. The sum of radiative and conductive losses has been estimated to be less than 9% of input electrical power at the higher air flow rate and less than 14% at the lower air flow rate.

Tests were repeated, for the same air flow rate, changing the input power such that the colors moved and other LC images were captured and processed until the heat transfer coefficient was calculated, through Eq. (1), over the entire heated surface.

Friction factor f was calculated from the conventional definition [31]

$$f = |dP/dx| D/\left(2\rho U^2\right) \quad (2)$$

on the basis of pressure gradient dP/dx measured by performing tests without heating. In Eq. (2), U is the mean air velocity and $D = 2\,W\,H\,/(W+H)$ is the hydraulic diameter of the channel.

Nusselt and Reynolds numbers were evaluated as

$$Nu = hD/k \quad (3)$$

$$Re = UD/\nu \quad (4)$$

where k and ν are the thermal conductivity and the kinematic viscosity of air, respectively. Experiments have been conducted for two values of the Reynolds number, namely $Re = 10000$ and 20000.

The Nusselt number was locally evaluated or regionally averaged (indicated as $\overline{Nu}$) over the heat transfer area from the 10th to the 13th heated module, significantly far from the entrance of the heated test section. Since the aim of this research was to identify an enhanced geometry able to increase the thermal performance of standard angled ribs in a high aspect ratio rectangular channel, local and averaged results obtained for the enhanced geometry (angled ribs with one or two intersecting ribs) were normalized by the values f_b and Nu_b (or $\overline{Nu}_b$) obtained for the baseline rib configuration (the standard angled ribs).

In order to quantify the thermal performance based on both the heat transfer coefficient augmentation and the frictional loss penalty and expressing the increased heat transfer for constant pumping power, a thermal performance index η has been introduced according to the expression reported in Ref. [32]

$$\eta = \frac{\left(\overline{Nu}/\overline{\mathrm{Nu}}_{\mathrm{b}}\right)}{\left(f/f_b\right)^n} \quad (5)$$

where the exponent n is related to the structure of the power-law representations giving the friction factor and the average Nusselt number for the baseline rib configuration as a function of the Reynolds number (here not known since only two Re values were explored).

The uncertainty estimation (at the 95% confidence level) of experimental measurements was performed according to the procedure outlined by Moffat [33]. The uncertainty in the Nusselt number, performed by taking into account errors associated with temperature (by LCs and thermocouples) readings, voltage and current measurements, and calculation of conductive and radiative losses, turned out to be ± 9%. Effects of streamwise and spanwise heat conduction, which could alter the UHF heating condition, were not accounted for; however, they have been minimized due to the small thickness (0.5 mm) and low thermal conductivity (0.30 W/m K) of the Vetronite layer that separates the electric track of the heater from the wall-to-fluid interface. The Reynolds number and the friction factor had a calculated uncertainty of ± 6% and ± 14%, respectively.

4. Computational simulations

Numerical simulations were performed with the main purpose of gaining information about the flow field and vortex structure, not investigated by experiments. The Fluent 16.2, finite-volume, commercial CFD code [34] was used for the numerical investigations. A structured grid has been created by a mesh generator inside the computational domain, encompassing the entire ribbed (unheated and heated) test section. The air flow was assumed to be incompressible, steady, turbulent and with constant thermophysical properties (taken at the temperature of 27°C). Simulations have been carried out by using the renormalization group (RNG) k-ε turbulent model. Two different Reynolds numbers were considered, namely $Re = 10000$ and 20000. The inlet turbulence intensity upstream of the ribbed channel was set equal to 4%, consistent with the mid-channel average axial turbulence intensity measured (by a hot-wire single probe Dantec 55P11) 125 mm upstream of the ribbed test section entrance.

The structured mesh of the domain was sufficiently refined in the vicinity of the solid boundaries to make y^+ values lower than 1.0. A grid independence analysis was conducted for a representative case (the standard angled ribs at $Re = 10000$) by progressively varying (along the three coordinates) the number of cells inside each model (and in the entire computational domain). The calculated Nusselt number averaged over a given repetitive module (No.12) and over the entire heated surfaces (average among all modules) showed a variation smaller than 0.6% passing from 9.3×10^5 to 1.3×10^6 cells inside the repetitive module; therefore, the mesh with 9.3×10^5 cells per module was selected in this study. The adopted structured mesh around each rib (side and top views) is shown in Fig. 4.

A uniform heat flux equal to 1000 W/m^2 was applied at the wall-to-fluid interface over each inter-rib module in the ribbed heated test section. Other solid boundaries, including rib surfaces, smooth channel walls, and ribbed unheated test section were considered as adiabatic.

5. Results and discussion

Fig. 5 shows typical examples of LC images, taken for the three rib arrangements, and the corresponding interpretation in terms of dimensionless heat transfer coefficient (Nusselt number). Data refer to a module sufficiently far from the entrance and $Re = 10000$. As previously explained, more LC images, for the same surface region and mass flow rate, were needed to reconstruct the heat transfer coefficient map over the whole area of interest.

Experimental Nusselt number contours for the entire heated section and all the three rib configurations are plotted in Fig. 6. For the sake of brevity, experimental results are reported only for $Re = 10000$, since results for $Re = 20000$ were qualitatively similar.

Results show significant spanwise variations of the Nusselt number for the standard angled ribs. When only angled ribs are present, vortices moving along the rib profiles (which will be shown in the following figures) bring relatively fresh air from the top to the bottom side wall, where the highest heat transfer coefficients are recorded. Conversely, the opposite region, close to the top side, is characterized by relatively low values of the heat transfer coefficient. The presence of one longitudinal rib that bisects the angled ribs leads to the breaking of the main secondary vortex into two secondary vortices. As a consequence, relatively high heat transfer coefficients are established in the bottom region of each sub-module, immediately downstream of each angled rib, while relatively low heat transfer coefficients persist over the opposite top region. When two intersecting ribs are installed, three sub-modules are originated and more secondary vortices are induced, leading again to local heat transfer enhancement close to the bottom region, downstream of the angled ribs, and to heat transfer reductions as the top region, upstream of the angled ribs, is approached. The redistribution of local heat transfer coefficient due to installation of intersecting ribs contributes to decrease spanwise variations, as inspection of Fig. 6 reveals at glance. It is worth noting that the iso-Nusselt contours over the two sub-modules originated from the installation of one intersecting rib and over the three sub-modules originated from the installation of two inter-

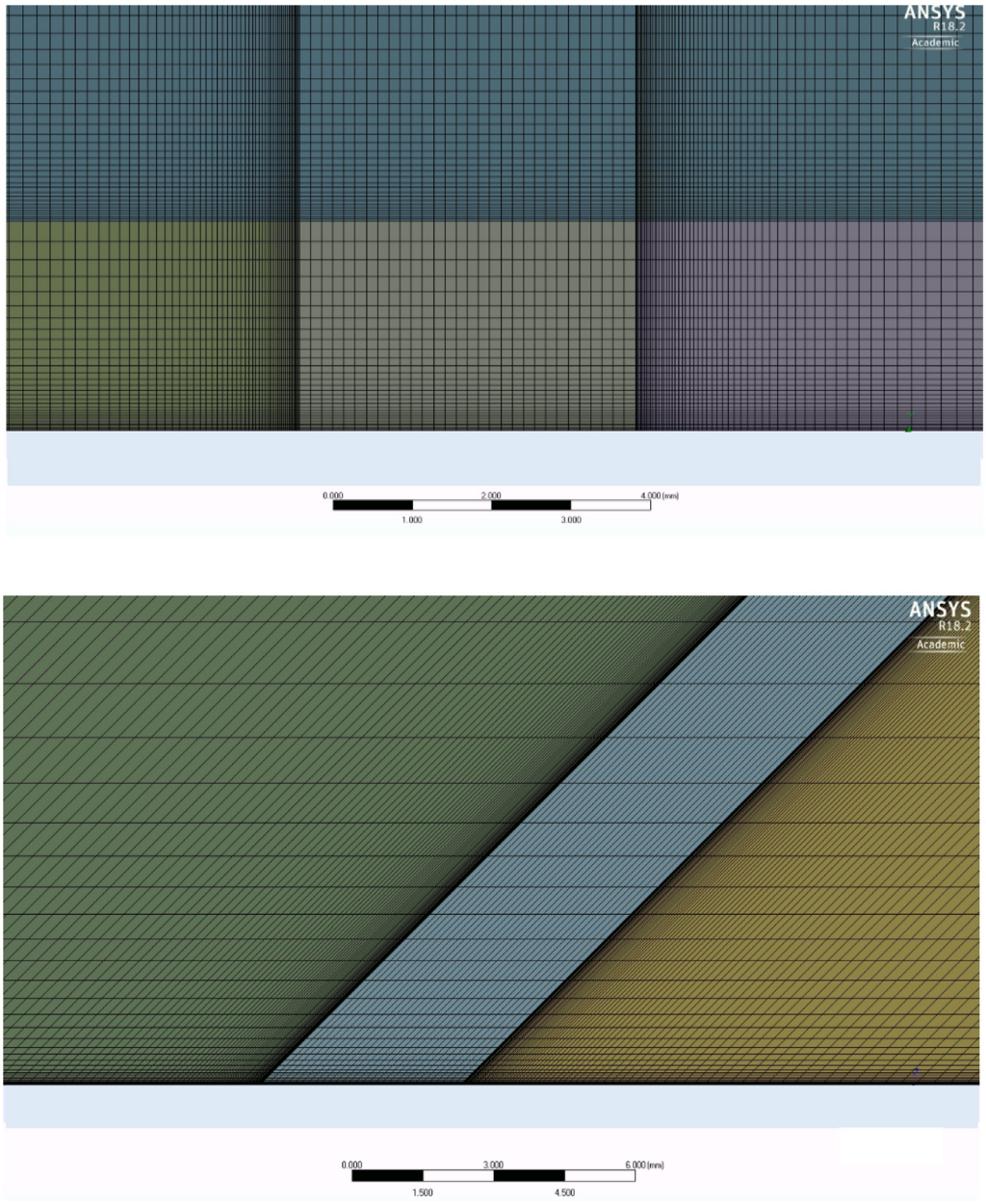

Fig. 4. The adopted structured mesh close to each rib (side and top views).

Table 1
Regionally averaged Nusselt numbers and friction factors obtained by experiments and numerical simulations.

Number of intersecting ribs	*Re*	f (exp.)	f (num.)	Differences (%)	$\overline{Nu}$ (exp.)	$\overline{Nu}$ (num.)	Differences (%)
0	10000	0.0288	0.0286	−0.7	82.5	78.0	−5.5
1	10000	0.0355	0.0348	−2.0	92.7	93.0	+0.3
2	10000	0.0425	0.0433	+1.9	97.1	94.5	−2.7
0	20000	0.0269	0.0275	+2.2	127.2	126.2	−0.8
1	20000	0.0330	0.0325	−1.5	144.6	142.0	−1.8
2	20000	0.0425	0.0405	−4.7	152.5	149.6	−1.9

secting ribs are similar in shape, but progressively higher values of Nusselt number are observed moving from the top to the bottom submodule.

Numerical distributions of Nusselt number were very similar to those obtained by experiments; therefore, the comparison between experimental and numerical results is provided in terms of friction factor and regionally averaged Nusselt number, as reported in Table 1. As previously mentioned, numerical simulations were performed only to infer information about flow field inside the channel; even though the comparison between numerical and experimental results is beyond the objective of this study, calculated friction factor and regionally averaged Nusselt number show good agreement with experimental data, with deviations within 5% for the friction factor and 6% for the Nusselt number, thus confirming the ability of CFD, using the RNG k-ε model, to capture the features of flow and heat transfer inside the ribbed channels.

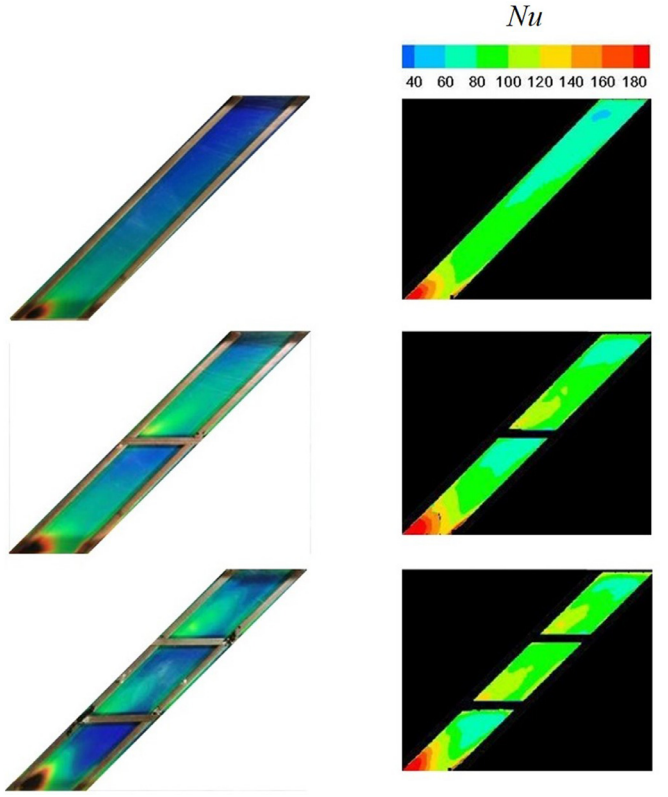

Fig. 5. Examples of liquid crystal images (left-hand side) and corresponding Nusselt number distributions (right-hand side) for the three rib configurations (Re = 10000).

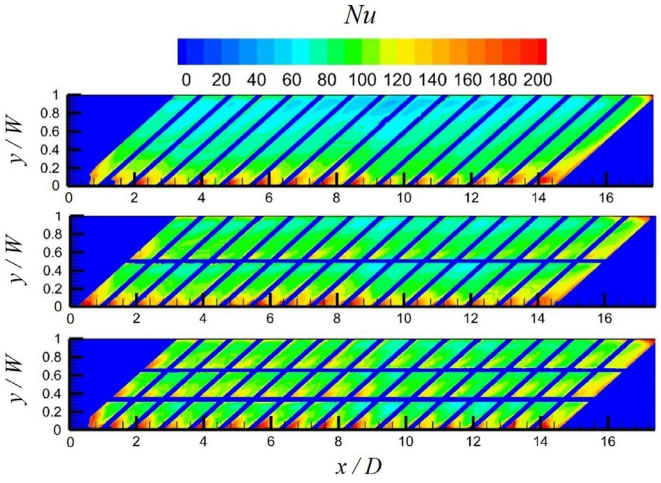

Fig. 6. Experimental Nusselt number contours for the three rib configurations (Re = 10000).

To further support the discussion above, and better explain the effects of the three different rib configurations on heat transfer, the flow field predicted by numerical simulations has been also inspected and presented in Figs. 7–9, where iso-vorticity surfaces, velocity vectors, and streamlines are reported, at Re= 10000, for the standard angled ribs (a), angled ribs with one intersecting rib (b) and with two intersecting ribs (c).

Fig. 7 shows an iso-vorticity surface properly selected for the purpose of marking the vortex between two adjacent ribs, adopting the same vorticity value for all of the cases considered. The configuration with only angled ribs installed clearly shows the presence of one vortex originating downstream of each rib in correspondence of the bottom side wall of the channel, which travels the inter-rib region reaching the downstream rib at larger y/W values. As previously discussed, the vortex flow has the effect of bringing cold air from the mainstream towards the heated wall in the region next to the bottom side wall of the channel, hence reducing the wall temperature in that region and increasing the local Nusselt number. As the vortex travels through the inter-rib region, its temperature is increased by the heated plate, with a consequent reduction of the Nusselt number as y/W is increased. When the inter-rib vortex encounters the top side wall, an upwash flow originates and a further motion travelling in the negative y/W direction near the wall opposite to the heated one occurs, followed by a downwash flow next to the bottom side wall. Consequently, a clockwise rotating (seen from upstream) streamwise helical vortex extending over the whole channel height is induced. This main flow secondary vortex can be clearly identified in Fig. 8, where the secondary velocity vectors evaluated in a cross-plane at x/D = 8.6 have been superimposed to the vorticity color plots, as well as in Fig. 9, where a limited number of streamlines properly selected to highlight the main flow secondary flow are depicted.

When one intersecting rib is installed in the middle of the channel, the secondary vortices (Fig. 7) in the inter-rib regions have a traveling distance limited to the respective sub-module width. The restarting of vortices at each junction between the intersecting and angled ribs provides the locally enhanced heat transfer coefficients previously noted. For this rib configuration, instead of one single main secondary vortex as in the case without intersecting ribs, a pair of counter-rotating streamwise helical vortices appears, as shown by both secondary vectors (Fig. 8) and streamlines (Fig. 9). In particular, Fig. 8 highlights the two downwash flows, one on the right and the other in the middle of the figure just on the left of the intersecting rib, which are the main responsible for the Nusselt number enhancement previously shown.

As the number of intersecting ribs has doubled, three different inter-rib secondary vortices occur in the spanwise direction, one for each sub-module created by the intersecting rib. In particular, the comparison of plots displayed in Fig. 7 shows that as the number of intersecting ribs, and consequently of inter-rib secondary vortices, increases, a larger portion of the module is interested by larger vorticity values, as demonstrated by the shape of the iso-vorticity surfaces, giving rise to a more uniform distribution of the vorticity in the spanwise direction. Moreover, for the case with two intersecting ribs, three large-scale main flow secondary flows are evident throughout the duct (Figs. 8 and 9). Even for this rib configuration, the downwash flows highlighted by the flow field analysis explain the physics, which regulates the heat transfer phenomena induced by the three different rib configurations.

Figs. 10–13 show the experimental distributions of the local Nusselt number ratio along the streamwise direction, for Re = 10000 and 20000, from 9.5 to 13.0 hydraulic diameters downstream of the entrance of the ribbed heated section. When a single intersecting rib is inserted in the channel, the Nusselt number evaluated close to the bottom side (y/W = 0.25, Fig. 10) has only limited variations (±10%) with respect to the baseline rib configuration for both Re values, since the main secondary vortex has not split into two secondary vortices yet. Conversely, close to the top side (y / W = 0.75, Fig. 11), significant heat transfer enhancements (from +15 to +40%) are achieved due to the vortex duplication, shown in Fig. 8(b), induced by the intersecting rib. The second vortex seems to produce, for both the investigated Re values, the largest heat transfer augmentation at about one third distance downstream of the inclined rib and the smallest augmentation as the upstream rib is approached.

Local results obtained for two equally spaced intersecting ribs are presented in Fig. 12 for Re=10000 and in Fig. 13 for Re=20000.

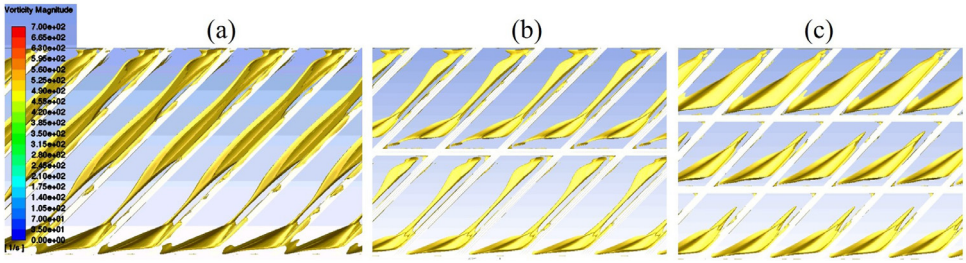

Fig. 7. 3D visualization (by means of an iso-vorticity surface) of the secondary flows between the ribs for the three configurations: (a) standard angled ribs, (b) angled ribs with one intersecting rib, (c) angled ribs with two intersecting ribs.

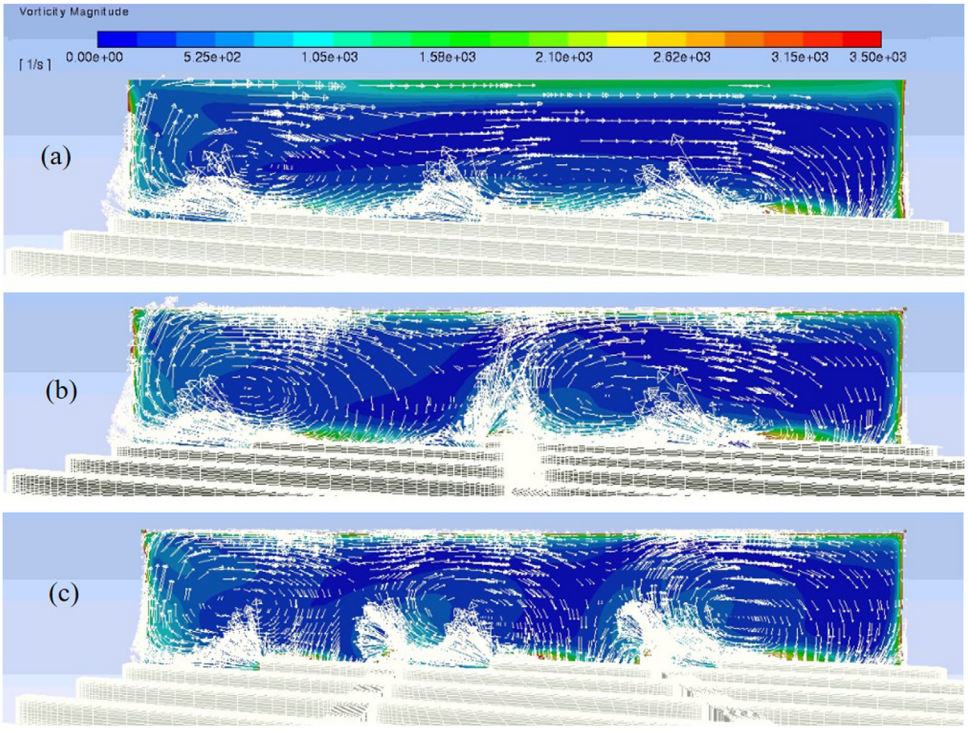

Fig. 8. Vorticity color plots in a cross-plane ($x/D = 8.6$) with secondary velocity vectors superimposed for the three configurations: (a) standard angled ribs, (b) angled ribs with one intersecting rib, (c) angled ribs with two intersecting ribs.

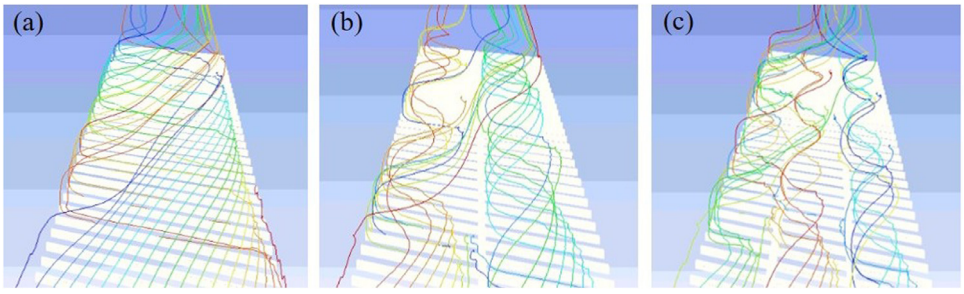

Fig. 9. 3D visualization of selected streamlines for the three configurations: (a) standard angled ribs, (b) angled ribs with one intersecting rib, (c) angled ribs with two intersecting ribs.

Nusselt number ratios for the two Reynolds numbers are quantitatively and qualitatively similar; as for the previous case, limited heat transfer coefficient variations, with respect to the standard angled ribs, are found close to the bottom side ($y / W = 0.16$), while a noticeable heat transfer enhancement is recorded in the central region ($y / W = 0.50$), due to the second secondary vortex, and especially close to the top side ($y / W = 0.84$), where the effect of the three secondary vortices generated by the intersecting ribs and observed in Fig. 8(c) is more pronounced. Again, the degree of the heat transfer augmentation induced by the intersecting ribs is sensitive to the streamwise position inside each inter-rib region, with peaks (up to +80% for $y / W = 0.84$) followed by a less marked enhancement (+ 30% for $y / W = 0.84$) as the streamwise coordinate increases.

Fig. 14 shows the enhancement induced by one or two longitudinal ribs in the normalized friction factor and in the normalized, regionally averaged, Nusselt number, for both $Re = 10000$ and 20000. For the sake of clarity, only experimental results are

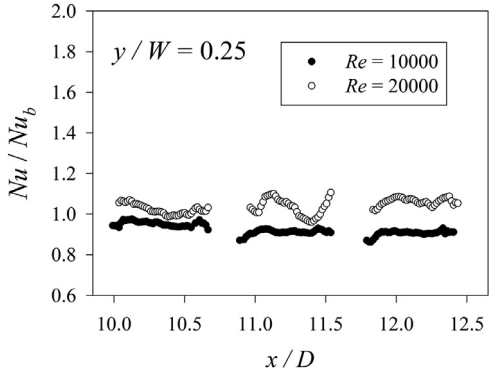

Fig. 10. Experimental distributions of Nusselt number (normalized by that for standard angled ribs) along the streamwise coordinate $y/W = 0.25$ for the channel with one intersecting rib (Re = 10000 and 20000).

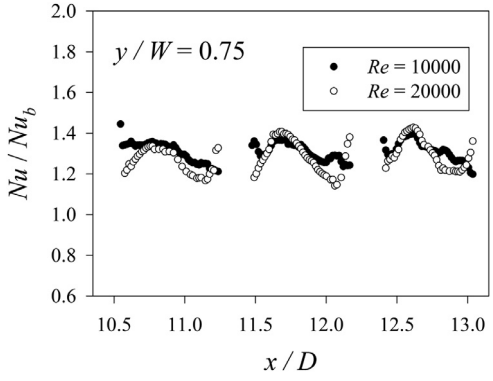

Fig. 11. Experimental distributions of Nusselt number (normalized by that for standard angled ribs) along the streamwise coordinate $y/W = 0.75$ for the channel with one intersecting rib (Re = 10000 and 20000).

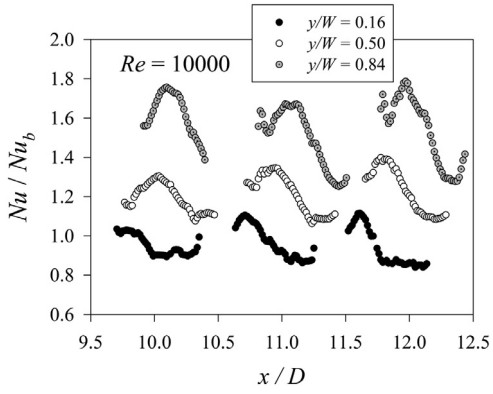

Fig. 12. Experimental distributions of Nusselt number (normalized by that for standard angled ribs) along the streamwise coordinates $y/W = 0.16$, 0.50, and 0.84, for the channel with two intersecting ribs; Re = 10000.

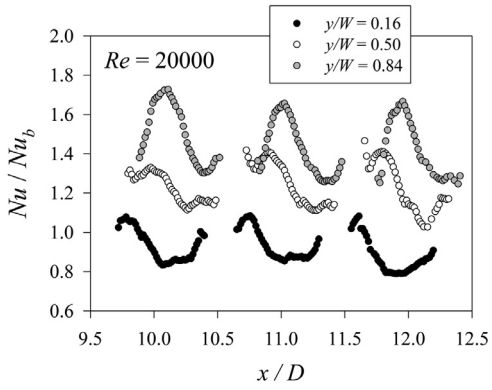

Fig. 13. Experimental distributions of Nusselt number (normalized by that for standard angled ribs) along the streamwise coordinates $y/W = 0.16$, 0.50, and 0.84, for the channel with two intersecting ribs; Re = 20000.

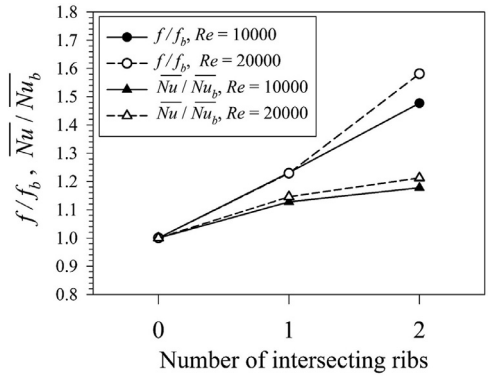

Fig. 14. Friction factor and regionally averaged Nusselt number (normalized by those for standard angled ribs) with one or two intersecting ribs. Experimental results for Re = 10000 and 20000.

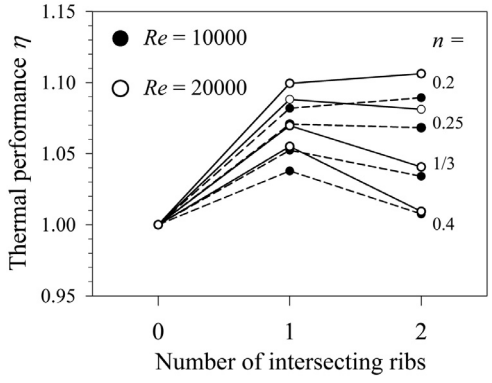

Fig. 15. Thermal performance (relative to the baseline configuration of standard angled ribs), based on Eq. (5), with one or two intersecting ribs.

reported (numerical results similarly behave). Assuming the standard angled rib configuration to be the baseline condition, one intersecting rib leads to about a 1.2-fold increase in pressure drop penalty, while two intersecting ribs produce a larger (1.5−1.6-fold) increase. At the same time, the intersecting ribs yield heat transfer enhancement compared with the standard angled ribs; the increase in normalized, regionally averaged, Nusselt number is about 1.15-fold for one intersecting rib and about 1.2-fold for two intersecting ribs.

When the frictional losses are coupled with the heat transfer enhancement according to the constraint of the same pumping power, the relative thermal performance can be evaluated according to Eq. (5). As shown in Fig. 15, the thermal performance is sensitive to the exponent n and, only in a minor part, to Reynolds number. Generally speaking, the thermal performance, relative to the standard angled rib configuration, turns out to increase, when one intersecting rib is present, for both Re values with enhancements up to +10%. When a second intersecting rib is installed, thermal performance remains stable or even decreases, depending on the assumed value of n. For n =1/3 (typical literature value, e.g., Refs. [14,16,18], where a smooth, unribbed channel was taken as reference configuration), Fig. 15 shows that inclined ribs with a single intersecting rib perform better than the case with two intersecting ribs, for both Re values. It is conjectured that passing from

one to two intersecting ribs leads to a slight increase in heat transfer, which is counterbalanced by a larger increase in pressure drop and a consequent slight reduction in thermal performance.

6. Conclusions

A rectangular channel (aspect ratio $AR = 5$) with 45 deg angled ribs on one side has been experimentally and numerically investigated in terms of heat transfer coefficients and friction factors. The presence of one and two longitudinal ribs (intersecting ribs) has been considered for the purpose of increasing the thermal performance with respect to the standard angled rib configuration.

When one or two intersecting ribs are present, additional vortices between ribs are generated at intersection points between the angled and the intersecting ribs, as outlined by numerical simulations. These additional vortices lead to increased values of both friction and heat transfer coefficient with respect to the standard angled ribs.

If the standard angled rib configuration is assumed to be the reference condition, one intersecting rib leads to an increase in the friction factor ratio of about 1.2-fold for one intersecting rib and of 1.5−1.6-fold for two intersecting ribs; the Nusselt number ratio enhancement due to the installation of intersecting ribs is about 1.15-fold for one intersecting rib and about 1.2-fold for two intersecting ribs.

The thermal performance based on the same pumping power is maximized when only one intersecting rib is considered. The installation of two intersecting ribs yields a little heat transfer increase, with respect to the case of a single intersecting rib, counterbalanced by a larger increase in pressure drop.

Funding

This research did not receive any specific grant from funding agencies in the public, commercial, or not-for-profit sectors.

Declaration of Competing Interest

The authors declare that they have no known competing financial interests or personal relationships that could have appeared to influence the work reported in this paper.

References

[1] J.C. Han, S. Dutta, S. Ekkad, Gas Turbine Heat Transfer and Cooling Technology, second ed., CRC Press, Boca Raton, 2012.
[2] A. Kumar, R.P. Saini, J.S. Saini, Heat and fluid flow characteristics of roughened solar air heater ducts–a review, Renew. Energy 47 (2012) 77–94.
[3] Q. Esmaili, A.A. Ranjbar, S. Porkhial, Experimental analysis of heat transfer in ribbed microchannel, Int. J. Therm. Sci. 130 (2018) 140–147.
[4] T. Ma, Q.W. Wang, M. Zeng, Y.T. Chen, Y. Liu, V. Nagarajan, Study on heat transfer and pressure drop performances of ribbed channel in the high temperature heat exchanger, Appl. Energy 99 (2012) 393–401.
[5] W. Zuo, J. E, H. Liu, Q. Peng, X. Zhao, Z. Zhang, Numerical investigations on an improved micro-cylindrical combustor with rectangular rib for enhancing heat transfer, Appl. Energy 184 (2016) 77–87.
[6] J.C. Han, L.R. Glicksman, W.M. Rohsenow, An investigation of heat transfer and friction for rib-roughened surfaces, Int. J. Heat Mass Transf. 21 (8) (1978) 1143–1156.
[7] J.C. Han, J.S. Park, C.K. Lei, Heat transfer enhancement in channels with turbulence promoters, ASME J. Eng. Gas Turbines Power 107 (3) (1985) 628–635.
[8] J.C. Han, J.S. Park, Developing heat transfer in rectangular channels with rib turbulators, Int. J. Heat Mass Transf. 31 (1) (1988) 183–195.
[9] J.C. Han, S. Ou, J.S. Park, C.K. Lei, Augmented heat transfer in rectangular channels of narrow aspect ratios with rib turbulators, Int. J. Heat Mass Transf. 32 (9) (1989) 1619–1630.
[10] J.S. Park, J.C. Han, Y. Huang, S. Ou, R.J. Boyle, Heat transfer performance comparisons of five different rectangular channels with parallel angled ribs, Int. J. Heat Mass Transf. 35 (11) (1992) 2891–2903.
[11] J.C. Han, Y.M. Zhang, C.P. Lee, Augmented heat transfer in square channels with parallel, crossed, and V-shaped angled ribs, ASME J. Heat Transf. 113 (3) (1991) 590–596.
[12] S.Y. Won, P.M. Ligrani, Comparisons of flow structure and local Nusselt numbers in channels with parallel- and crossed-rib turbulators, Int. J. Heat Mass Transf. 47 (8−9) (2004) 1573–1586.
[13] R.T. Kukreja, S.C. Lau, R.D. McMillin, Local heat/mass transfer distribution in a square channel with full and V-shaped ribs, Int. J. Heat Mass Transf. 36 (8) (1993) 2013–2020.
[14] M.E. Taslim, T. Li, D.M. Kercher, Experimental heat transfer and friction in channels roughened with angled, V-shaped, and discrete ribs on two opposite walls, ASME J. Turbomach. 118 (1) (1996) 20–28.
[15] S.V. Ekkad, J.C. Han, Detailed heat transfer distributions in two-pass square channels with rib turbulators, Int. J. Heat Mass Transf. 40 (11) (1997) 2525–2537.
[16] X. Gao, B. Sundén, Heat transfer and pressure drop measurements in rib-roughened rectangular ducts, Exp. Therm. Fluid Sci. 24 (1−2) (2001) 25–34.
[17] G. Tanda, Heat transfer in rectangular channels with transverse and V-shaped broken ribs, Int. J. Heat Mass Transf. 47 (2) (2004) 229–243.
[18] L.M. Wright, W.L. Fu, J.C. Han, Thermal performance of angled, V-shaped, and W-shaped rib turbulators in rotating rectangular cooling channels (AR=4:1), ASME J. Turbomach. 126 (4) (2004) 604–614.
[19] D.H. Lee, D.H. Rhee, K.M. Kim, H.H. Cho, H.K. Moon, Detailed measurement of heat/mass transfer with continuous and multiple V-shaped ribs in rectangular channel, Energy 34 (11) (2009) 1770–1778.
[20] J.C. Han, Y.M. Zhang, High performance heat transfer ducts with parallel broken and V-shaped broken ribs, Int. J. Heat Mass Transf. 35 (2) (1992) 513–523.
[21] H.H. Cho, S.J. Wu, H.J. Kwon, Local heat/mass transfer measurements in a rectangular duct with discrete ribs, ASME J. Turbomach. 122 (3) (2000) 579–586.
[22] H.H. Cho, Y.Y. Kim, D.H. Rhee, S.Y. Lee, S.J. Wu, C. Choi, The effects of gap position in discrete ribs on local heat/mass transfer in a square duct, J. Enhanc. Heat Transf. 10 (3) (2003) 287–300.
[23] K.R. Aharwal, B.K. Gandhi, J.S. Saini, Heat transfer and friction characteristics of solar air heater ducts having integral inclined discrete ribs on absorber plate, Int. J. Heat Mass Transf. 52 (25−26) (2009) 5970–5977.
[24] A. Chaube, S. Gupta, P. Verma, Heat transfer and friction factor enhancement in a square channel having integral inclined discrete ribs on two opposite walls, J. Mech. Sci. Technol. 28 (5) (2014) 1927–1937.
[25] H. Chung, J.S. Park, S. Park, S.M. Choi, D.H. Rhee, H.H. Cho, Augmented heat transfer with intersecting rib in rectangular channels having different aspect ratios, Int. J. Heat Mass Transf. 88 (2015) 357–367.
[26] A. Afzal, H. Chung, K. Muralidhar, H.H. Cho, Neural-network-assisted optimization of rectangular channels with intersecting ribs for enhanced thermal performance, Heat Transf. Eng. 41 (18) (2020) 1609–1625.
[27] L. Baggetta, F. Satta, G. Tanda, A possible strategy for the performance enhancement of turbine blade internal cooling with inclined ribs, Heat Transf. Eng. 40 (1−2) (2019) 184–192.
[28] G. Tanda, R. Abram, Forced convection heat transfer in channels with rib turbulators inclined at 45 deg, ASME J. Turbomach. 131 (2) (2009) 021012.
[29] G. Tanda, Effect of rib spacing on heat transfer and friction in a rectangular channel with 45° angled rib turbulators on one/two walls, Int. J. Heat Mass Transf. 54 (5−6) (2011) 1081–1090.
[30] F. Satta, G. Tanda, Measurement of local heat transfer coefficient on the endwall of a turbine blade cascade by liquid crystal thermography, Exp. Therm. Fluid Sci. 58 (2014) 209–215.
[31] A. Bejan, Heat Transfer, Wiley, New York, 1993.
[32] J.F. Fan, W.K. Ding, J.F. Zhang, Y.L. He, W.Q. Tao, A performance evaluation plot of enhanced heat transfer techniques oriented for energy-saving, Int. J. Heat Mass Transf. 52 (1−2) (2009) 33–44.
[33] R.J. Moffat, Describing the uncertainties in experimental results, Exp. Therm. Fluid Sci. 1 (1988) 3–17.
[34] Fluent inc. Fluent user's guide, version 16.2, 2015.